CHAPTER 4

DETERMINATION OF ASPECT RATIO OF ANISOMETRIC TALC PARTICLES FROM PARTICLE SIZE ANALYSIS

4.1- Introduction

The final shape of natural minerals as raw materials is determined by its genesis, by its chemistry, its crystal structure and by the grinding processing it has undergone [1]. The mineral rupture involves several different processes occurring together or successively. As an approximation, during the comminution of phyllosilicates, two distinct breakage processes occur: the breakage is parallel to ***c***-axis, i.e., across the platelet; covalent/ionic bonds are broken in this process which is termed **fracture;** the breakage is perpendicular to the ***c***-axis, i.e., along the flake basal plane and do not theoretically break covalent bonds. This phenomenon is termed **delamination**, and the energy spent to produce it is exceptionally lower than the fracture energy. In the case of kaolinite the delamination energy (E_d) is only 25% of fracture energy (E_f) [2, 3], as shown in Figure 4.1.

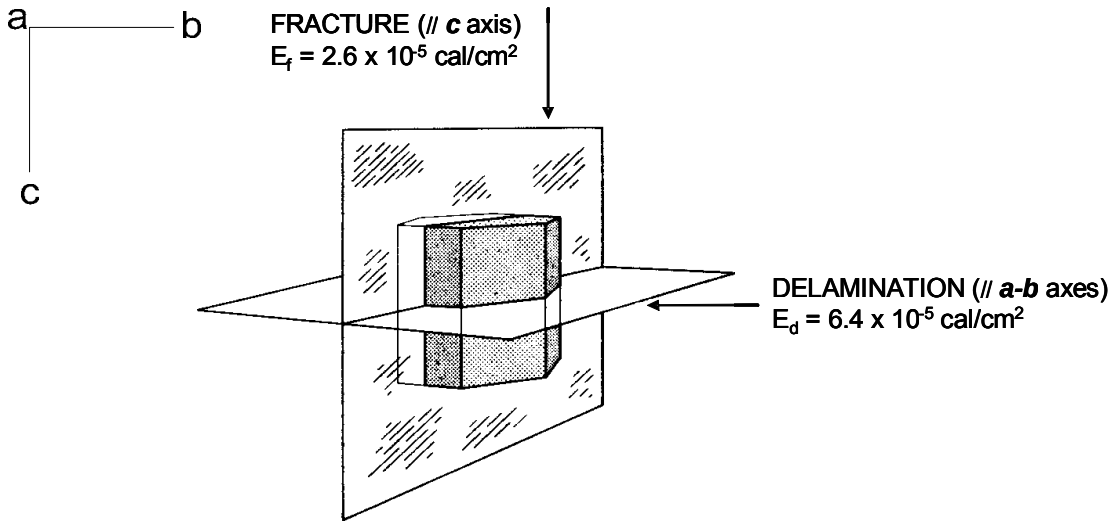

Figure 4.1. Crystallographic cleavage energy planes in kaolinite. The delamination energy is related to the break of hydrogen bonds whereas the fracture energy is related to the break of covalent bonds, which explains their difference in magnitude.

It must be emphasized that the numbers shown in Figure 4.1 are for the kaolinite ideal crystal structure and they do change in the case of isomorphic substitution within the crystal lattice. This observation applies to any other sheet silicate.

To the best of our knowledge the delamination/fracture energy data for talc were not found on literature. However, it can be assumed that its delamination energy is lower than that of kaolinite since the layers are held together by van der Waals forces, which are weaker than hydrogen bonds, and very readily cleave along the crystallographic ***c*** direction when an external stress is applied. Although occurrence of weak van der Waals bonds along the planes favors cleavages along (a-b) plane, grinding equipment and operating parameters are known to affect the mode of comminution in terms of dominance of delamination over fracture. It is well established that different mills are designed to apply the force in different ways. Comminution techniques that can maximize the delamination and then increase the aspect ratio (R) of lamellar-shaped particles can improve properties of clay minerals used as fillers or pigments in paper, polymers, elastomers, paints, ceramics and cosmetics.

4.2- Definition of aspect ratio and its practical importance

Due to the lamellar habit of the mineral talc, after comminution, the resulting particles normally have the flaky or disc-like morphology. The mathematical model adopted to represent the plate-like or disc-like talc particles was of an oblate spheroid (Figure 4.2). An oblate spheroid (“flattened sphere”) is a surface of revolution obtained by rotating an ellipse about its minor axis [4].

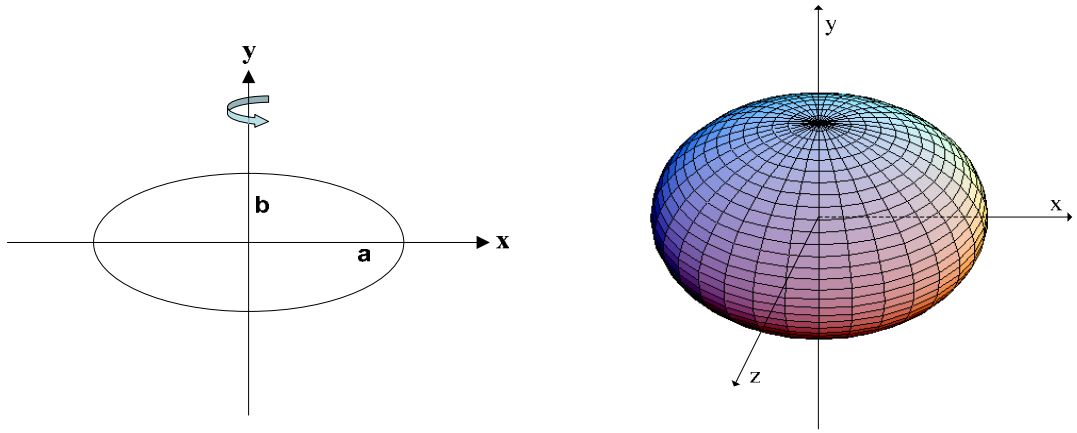

a) b)

Figure 4.2. The oblate spheroid (b) is the body obtained by allowing the ellipse (a) with major axis *a* and minor axis *b* to rotate around its minor axis.

The shape of lamellar minerals is commonly expressed as its aspect ratio (R), but others shape descriptors are also available [5, 6]. For anisometric particles such as discs it is defined as the ratio of the basal plane's biggest diameter, *a*, to its thickness, *b*. Using the notation presented on Figure 4.2 one can determine:

$$\mathrm{R} = \frac{a}{b} \tag{4.1}$$

There has been much interest in recent times in measuring the size and aspect ratio of small, micrometer or sub-micrometer, particles. The priority assigned to the topic results from the fact that the subject is of more than academic importance. Powdered materials of micron size are widely used in materials science and engineering. The size and shape distributions of particles will affect the way in which particles pack, fluidize, sediment, break, flow and agglomerate [7] which in turn affect the performance of the mineral in its final application. Mineral fillers are major components of paints, rubbers, plastics of various kinds, papers, cosmetics and ceramics, just to name a few.

Particle shape is, for example, an important factor determining the use of fillers in plastics. There have been a number of theories concerning the reinforcement of plastics

with plate-like materials which attribute the degree or extent of reinforcement to the average aspect ratio of the flake. These studies have shown that particle shape is very important in determining the stiffness, or rigidity [8, 9], of a composite, the heat distortion temperature [10], the flow and rheology of a melt or liquid [11], impact strength [12], yield stress [13] and gas barrier properties [14], i.e., many of the important properties of a composite. Indeed, most of the current predictive equations for the properties of filled composites use shape and size factors. For example, Nielsen [10], by modifying the Halpin-Tsai equation, showed that the relative modulus in a particulate-filled composite can be estimated by using equation (4.2).

$$\frac{E_c}{E_m} = \frac{1 + AB\phi_2}{1 - B\psi\phi_2} \tag{4.2}$$

where

$$A = k_E - 1, \qquad B = \frac{E_f / E_m - 1}{E_f / E_m + A} \qquad \text{and} \qquad \psi = 1 + \left(\frac{1 - P_f}{P_f^2}\right)\phi_2$$

E_c, E_m and E_f are moduli of the composite, matrix and filler, respectively; Φ_2 is the filler volume fraction; and P_f is the maximum packing fraction of the filler; k_E is the Einstein coefficient. The Einstein coefficient, in turn, is directly proportional to the filler aspect ratio (R) and consequently, the higher the value of R, the higher k_E and the higher the composite modulus (M). Recently, other models correlating the Young's modulus and the aspect ratio of the reinforcement have been proposed [15].

Another important application for lamellar clay minerals such as talc and kaolin is in the paper industry either as filler or as an ingredient of paper coating. For both applications it is paramount to determine the aspect ratio of the fillers being used since it has an important role during the paper processing and in the final application (printing) as well. Platy fillers give papers with higher gloss and lower porosity (and hence better printing properties), both attractive features [16]. In paper coating, the particle size and shape distributions have a direct impact on the rheological properties [17-19], runability

and final properties of the coating suspension [20]. Usually, pigments with higher R have a better degree of coverage and also improve gloss [21].

From the considerations made above, the importance of particle shape is now recognized in a great variety of industries and it became clear that there is a need to understand how to measure, control and manipulate particle shape. Nevertheless, characterization and measurement of shape is a difficult task since most powders of industrial importance are irregular in shape which is never well defined by only a few variables, especially in the case of anisometric talc particles.

There are several studies to determine particle shapes of clay minerals and other materials involving the use of microscopy-based and image analyses techniques [22-29]. Although measuring the aspect ratio by microscopy is direct and became fundamentally simple, it is associated with some problems and difficulties: to obtain a statistically valid number a large number of particles needs to be measured which is an extremely tedious, time-consuming and expensive task. In addition, it is very difficult to measure the thickness of this materials such as talc, and it becomes subjective when primary particles cannot be clearly distinguished form agglomerates [30].

Others techniques such as field-flow fraction combined with electron microscopy [31], image analysis and X-ray diffraction [32], solely laser diffractometry [33-36], Fourier Transform Infrared Spectroscopy (FTIR) [37], and profilometry combined with image analysis [38] have also been employed for the determination of aspect ratio of particles. Nonetheless, in this investigation the method originally proposed by Parslow and Jennings [39-41] for determination of the aspect ratio of minerals was adopted.

In particle size analysis, it is commonplace to analyze data for anisometric particles as if the particles were spheres and the resulting parameter is termed equivalent spherical diameter (ESD) [42]. A variety of physical phenomena have been used in various techniques and instruments as the basis for particle size measurement [43, 44]. The Parslow and Jennings method is based on the fact that the dependence of

the ESD on the major dimension and aspect ratio differs with the physical principle of the experimental method, and identity of the ESD values from different methods cannot be expected except for the case of purely spherical particles. When the particles are asymmetric the equivalent spherical diameters (ESD) will not equate between different techniques. Non-identity signifies non-sphericity and, consequently, one should be able to determine the aspect ratio by comparing the results from two or more sizing methods.

Since it was first proposed in 1986, the Parslow-Jennings method has been successfully used by several authors [30, 45-48] for the estimation of the aspect ratio of different minerals.

4.3- Particle size analysis – sedimentation and laser diffraction

Sedimentation and laser diffraction methods are among the most widely applied techniques for routine particle size analysis of minerals of industrial importance and they were chosen for the purpose of this investigation. This section intends to give a general review of the basic principles underlying each of the mentioned methods.

4.3.1- X-ray gravitational sedimentation

Gravitational sedimentation-based techniques are amongst the most commonly used techniques for particle size and size distribution determination. Instruments based on this type of technique are routinely used in industrial and research applications. The specific equipment used in this investigation was the Sedigraph 5100 particle size analyzer (Micromeritics, GA, USA).

The Sedigraph 5100 automatically determines particle size by the X-ray/sedimentation method, which measures the gravity-induced settling rates of different size particles in a liquid with known properties. (The particles will separate by settling velocity/size as they fall.) Using a collimated (parallel) low energy X-ray beam, it measures the change in concentration of particles remaining in aqueous suspension as

a function of time. Since the particles in the cell absorb X-rays, proportionally to their mass, only a percentage of the original X-ray beam reaches the detector. The X-ray source and detector assembly remain stationary, while the cell moves vertically between them. Consequently, the concentration of particle mass at various points in the cell affects the number of X-ray pulses reaching the detector. Thus, knowing the particle density and by determining the concentration of the particles at various depths, the settling velocities of the particles can be determined and the particle diameter corresponding to that velocity calculated via equation (4.7), shown below. Since the attenuation of X-radiation is proportional to the mass of the absorber, the particle size distribution is expressed as the cumulative mass percent versus equivalent spherical particle diameter [49]. The schematic drawing of X-ray gravitational sedimentation equipment is shown in Figure 4.3.

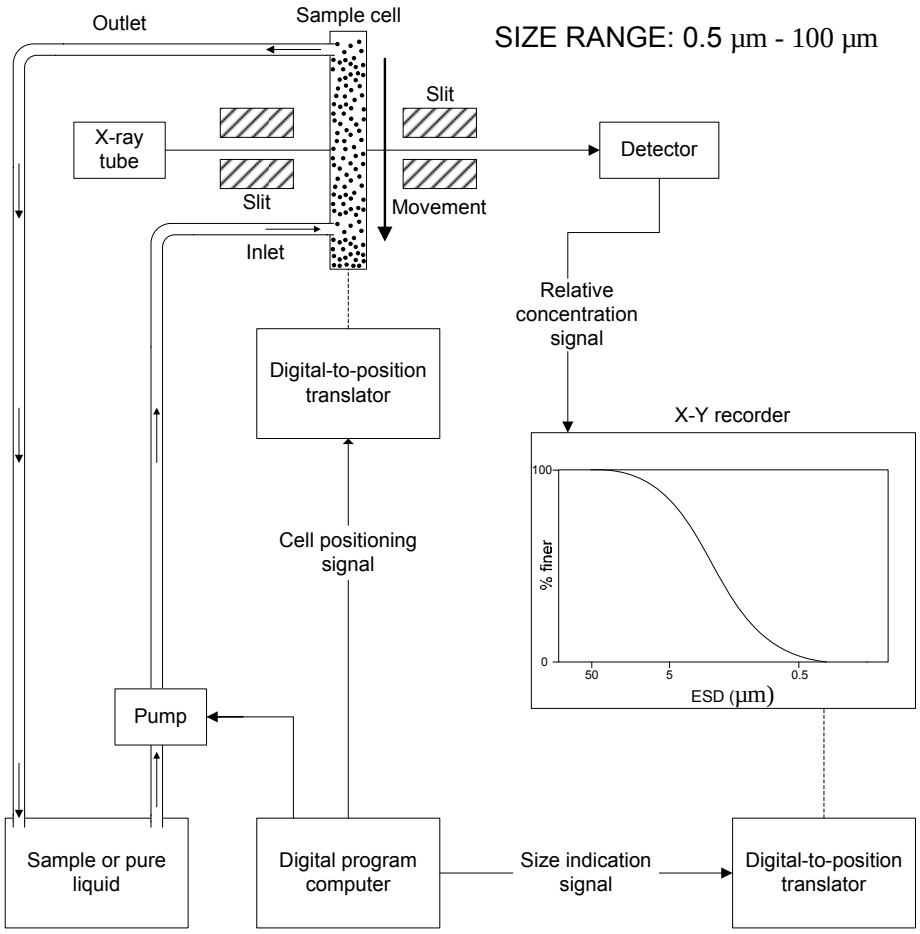

Figure 4.3. Schematic of a typical apparatus using the X-ray gravitational technique. Adapted from [50].

The driving force downwards, F_g, is the gravitational force such that for a spherical particle [43]:

$$F_g = m_p g = \frac{\pi}{6} d^3 \rho_s g \tag{4.3}$$

where m_p is the mass of the particle, g the acceleration due to gravity, d the diameter of the particle and ρ_s the density of the particle.

In the opposite direction, a lift force (Archimedean buoyancy force), F_L, is acting on the spherical particle in the liquid:

$$F_L = m_f g = \frac{\pi}{6} d^3 \rho_f g \tag{4.4}$$

where m_f is the mass of the same volume of fluid, g the acceleration due to gravity, d the diameter of the particle and ρ_f the density of the fluid.

Also in the opposite direction, a drag force (resistance force) F_D exerted by the viscous liquid is acting and for laminar settling it is given by the Stokes formula:

$$F_D = 3\pi\eta d\upsilon_{St} \tag{4.5}$$

where d is again the particle's diameter, η the viscosity of the fluid and υ_{St} the terminal settling velocity of the particle in the Stokes region.

By neglecting inertia terms, F_g and (F_D+F_L) must balance one another:

$$F_g - (F_D + F_L) = 0 \tag{4.6}$$

$$F_g = F_D + F_L \Rightarrow \upsilon_{St} = \frac{(\rho_s - \rho_f) g d^3}{18\eta d} = \frac{(\rho_s - \rho_f) g d_{St}^2}{18\eta} \tag{4.7}$$

where d_{St} is the Stokes' diameter.

Thus, according to Eq. (4.7) the terminal settling velocity of a spherical particle in a fluid is proportional to the square of the particle's diameter. This is called Stokes' law of settling. The Stokes' law is applicable, provided that the Reynold's number is less than 0.25, i.e., falls within the laminar flow region [51]. Under these conditions of flow, the terminal velocity is then assumed to be reached instantaneously and inertia terms can be neglected [43].

Thus, the size distribution of the settling particles is based on Stokes law of settling and the results are reported as the Stokes equivalent spherical diameters (ESD) of the particles, which is defined as the diameter of a sphere that has the same density and the same velocity as the particle in a fluid of the same density and viscosity settling under laminar flow conditions [52]. The typical size range for analysis is from about 0.5 μm to about 100 μm [53].

A successful sedimentation analysis therefore requires a reasonable difference in densities between the particles and the fluid, and a viscosity of the fluid that is not too high. Brownian motion will have a strong effect when analyzing particles finer than about 0.5 μm [54]. Depending upon the density and the size of this fine fraction, the random thermal motion can keep the particles from settling, leading to a skewed distribution indicative of a greater fine fraction than is actually present. The typical cumulative sedimentation curve will level out at the fine end of the size distribution, indicating a significant influence of Brownian motion. Allen [55, 56] describes the limits of the gravitational sedimentation methods relating to concentration limits, upper and lower size limits.

4.3.2- Laser diffraction

When light strikes on a small particle it gives rise to four different but inherently related scattering phenomena, namely, diffraction, refraction, reflection and absorption of the incident beam [54]. The magnitude of each phenomenon will vary depending

upon the nature and size of the particle and the beam. Size analysis by interpretation of the scattering light patterns formed due to diffraction of the incident light (usually a laser) is used as operational principle in many types of equipments. The specific equipment used in this investigation was the Malvern Mastersizer S (Malvern Instruments, Worcestershire, UK). The dynamic range of the instrument goes from 0.05 μm to 880 μm [57].

During the laser diffraction measurement, particles are passed through a focused laser beam (Figure 4.4). These particles scatter light at an angle that is inversely proportional to their size. The diffraction pattern formed is then measured by a series of photosensitive detectors and numerical values relating to the scattering pattern are then recorded for subsequent analysis. Using an appropriate optical model, these numerical scattering values are transformed to yield commonly the proportion of total volume to a discrete number of size classes forming a volumetric particle size distribution[1].

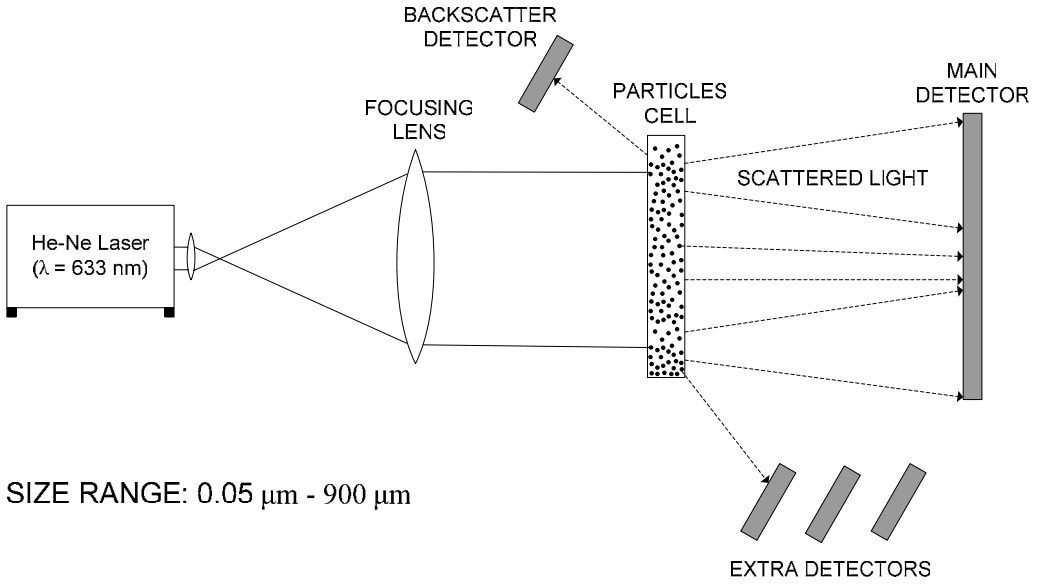

Figure 4.4. Schematic of the operational principle of the laser diffraction technique (courtesy of Malvern Instruments). The determination of a particle size distribution may be considered to have three stages.1) The light beam is scattered by particles and the resultant scattering pattern is recorded. 2) The pattern is converted into a digital signal. 3) The signal is inverted into a particle size distribution.

[1] If for example 11% of the distribution in the size category 5 – 10 μm this means that the total volume of all particles with diameters in this range represents 11% of the total volume of all particles in the distribution.

Typically either the Fraunhofer or Mie optical model is used to convert the scattering patterns into a particle size distribution though other models exist.

Historically, the Fraunhofer approximation was the basis for the first optical model employed for particle size measurement [58]. The model assumes sphericity of the particles, a relative refractive index higher than 1.2 and that the particles' diameters are much larger than the wavelength of the incident beam. Due to this latter prerequisite, the predominant scattering is caused by simple diffraction from the edges of the particles; this also means that the same scattering pattern is obtained as for thin two-dimensional circular discs [59] and the projected area distribution is assumed [42].

The Fraunhofer theory does not require any information about the optical properties (refractive index) of the material. In practice, the approximation is valid for coarse particles. If the particle size is larger than about 50 μm, then there is good robustness to RI changes, i.e. the RI has little effect on the deconvolution, and the Fraunhofer approximation gives good results. For particles smaller than about 50 μm, the Mie theory, that follows, offers the best solution. For medium sized particles (1 μm to 50 μm) with $n_p/n_m > 1.1$ and/or $n_i > 0.05$ the Fraunhofer approximation usually gives good results [59, 60]. Mackinnon *et al*. [61], in their work with kaolinite, concluded that particle sizes determined by laser diffraction must be calculated using Mie theory when the dominant particle size is less than about 5 μm.

The Mie scattering theory is a comprehensive and more rigorous mathematical solution to scattering of incident light by spherical particles and it is applicable when the particle size is equal to, or smaller than, the wavelength of the incident light. Mie also assumes the particles to be spherical. This theory indicates the necessity for a precise knowledge of the real and imaginary components of the refractive index of the material being analyzed, in order to accurately determine particle size and size distribution. The value of the real component of the refractive index can be found with relative ease, but determining the value of the imaginary component can be far more difficult. In the region

bellow 1 micrometer, scattering is usually weak but adsorption (imaginary component of the refractive index) is strong and it dominates.

Though there are various sources for obtaining the values of the refractive indices of materials [59, 62, 63], caution should be exercised while using them. The wavelength at which these values have been determined and reported may not be the same wavelength at which the instrument is operating and may thus introduce systematic errors. For materials that occur in different stable phases, the value used should correspond to that particular phase.

It is however, far more difficult to obtain the value of the imaginary component of the refractive index of the material which represents the amount of the incident electromagnetic energy that is absorbed and converted into others forms of energy, e.g. thermal energy [64]. Some tables exist for determination of these values, but often trial and error procedures of size determination using a microscopy-based technique and an instrument using laser diffraction have to be utilized [65]. A comprehensive text describing both Fraunhofer and Mie theories can be found in the book of Bohren and Huffman [64].

It is important to mention that the laser diffraction technique is not able do distinguish between primary particles and clusters of particles and the proper dispersion of the sample prior to the analysis is essential. In addition, without full dispersion the refractive index is a meaningless concept since the RI of agglomerates is different than that of primary particles [66]. An internationally accepted procedure for sample preparation is given by the International Organization for Standardization (ISO) [67].

Mie theory accounts for the passage of light through a particle whereas the Fraunhofer approximation assumes that the particle is an opaque thin disc. Thus, as mentioned before, Mie theory extracts volumes of particles and Fraunhofer a projected area for an irregular particle presenting all axes to the laser beam. Nonetheless, in the case of opaque thin particles, such as talc, they will not present all axes to the laser

beam since the particles tend to preferentially align in line with the direction of flow. Thus only the x and y axes will be presented to the laser beam and in this situation Mie will extract the sphere of same diameter as the cross-sectional projected area of the particle [66]. This same assumption was done by Inoue when applying the Parslow-Jennings method to measure the aspect ratio of kaolinite [30].

Most modern instruments based on laser light diffraction for particle size determination utilize Mie theory (with some proprietary variation) for modeling the diffraction patterns that are formed. The Malvern Mastersizer S has the flexibility to allow the user the selection of the optical model for the deconvolution of the scattered pattern. Some studies have been published comparing the results of Mie and Fraunhofer theories [68].

4.4- Determination of aspect ratio (R) from particle size analysis data: The Parslow-Jennings method

Using rigorous considerations from hydrodynamics, Parslow and Jennings [39], showed that the dimensions of an oblate spheroid settling with no preferential orientation could be directly related to the spherical Stokes' diameter through the following equation:

$$d_{Stokes} = \mathrm{a}\sqrt{\frac{\arctan^{-1}\sqrt{\mathrm{R}^2\text{-}1}}{\sqrt{\mathrm{R}^2\text{-}1}}} \tag{4.8}$$

where d_{Stokes} is the Stokes' equivalent spherical diameter for an oblate spheroid, *a* is the basal plane's biggest diameter and *R* is the particle's aspect ratio as defined by equation (4.1).

Similarly, they equated the projected area of an oblate spheroid in random orientation with that of a sphere and derived equation correlating the diameter of the spheroid with its length and aspect ratio [40], such that:

$$d_{Laser} = \frac{a}{\sqrt{2}} \sqrt{1 + \frac{\ln[R + (\sqrt{R^2 - 1})]}{R\sqrt{R^2 - 1}}} \qquad (4.9)$$

where d_{Laser} is the light scattering (projected area) equivalent spherical diameter for an oblate spheroid.

It can be inferred from equations (4.8) and (4.9) that, for these models, $d_{Stokes} \neq d_{Laser}$ since they have different dependence on aspect ratio. It follows that one cannot expect the laser diffraction and sedimentation to give the same diameter, except for the limiting case of spherical particles, i.e., for R = 1. Figure 4.5 presents these equations in graphical form. The ordinate was normalized by the major dimension, *a*, so as to express the ESD variation as a function of the aspect ratio alone.

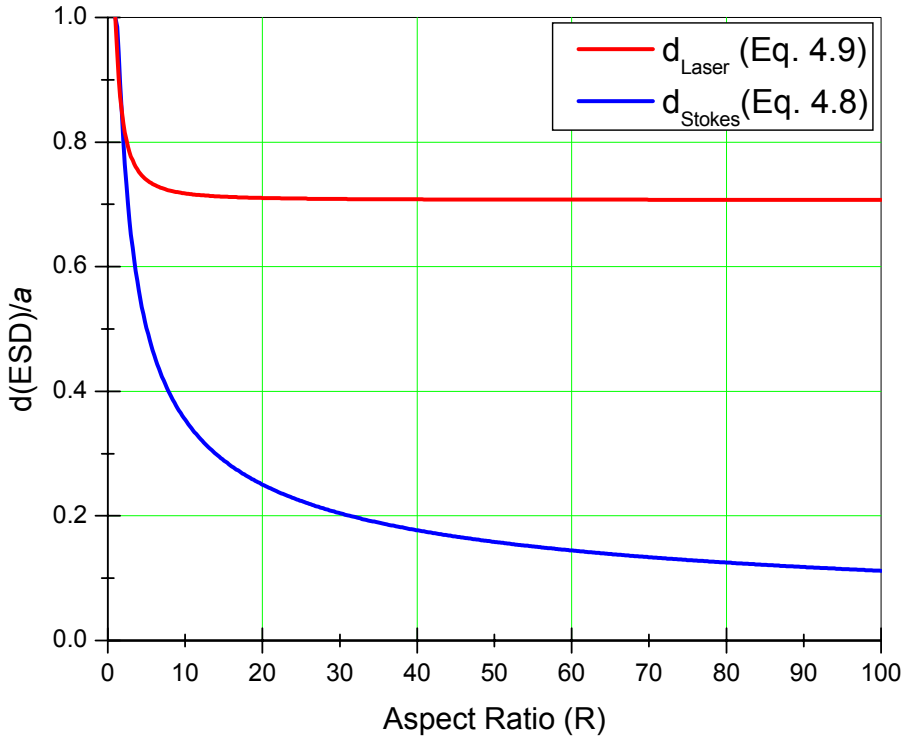

Figure 4.5. Oblate spheroid equivalent spherical diameters for laser diffraction and sedimentation techniques.

From figure 4.5 one can see that the bigger the aspect ratio the smaller the ratio d_{Stokes} / d_{Laser} and that as the aspect ratio approaches the unity the results from different

sizing techniques tend to converge. Another important observation is the fact that for anisometric particles, the equivalent spherical diameter is always less than the true major dimension, *a*, regardless of the physical principle being used for the particle size determination.

Eliminating the major axis *a* between equations (4.8) and (4.9) yields, after simplification, the working equation:

$$\left(\frac{D_{Stokes}}{D_{Laser}}\right) = \sqrt{\frac{2\mathrm{R}\arctan\sqrt{(\mathrm{R}^2-1)}}{\mathrm{R}\sqrt{(\mathrm{R}^2-1)}+\ln(\mathrm{R}+\sqrt{(\mathrm{R}^2-1)})}} \qquad (4.10)$$

The right-hand side of equation (4.10) contains only the variable R, which one seeks to determine. If the ratio at the left-hand side is close to unit it signifies near sphericity of the particle morphology whereas when it is lower than unit it indicates anisometric shapes.

The utility of the equations is as follows. With two types of sizing equipments available, the standard procedures are followed to obtain measurements of the particle size distribution by each method, which are expressed as weight cumulative distributions. One can compare the two ESD values form the two methods at any chosen equivalent percentage point on the two distribution curves and calculate a value for the aspect ratio. Usually, the two sets of data are compared at the central of 50% cumulative point and, in this case, the aspect ratio is referred to as the average aspect ratio. After determining the average aspect ratio, the average thickness, $\bar{b}$, of the particles can also be estimated.

More recently, Pabst and co-workers [69, 70] used light scattering (Fraunhofer theory) and sedimentation to extract shape information form particle size measurements when working with kaolin. The geometric model adopted was also the oblate or disc-like shaped particles. By replacing the volume of a sphere by the volume of a disc as a

function of its aspect ratio in equations (4.3) and (4.4) Pabst ended up with the following expressions for the gravitational and lift forces respectively:

$$F_g = m_p g = \frac{\pi d^3}{4R} \rho_s g \tag{4.11}$$

$$F_L = m_f g = \frac{\pi d^3}{4R} \rho_f g \tag{4.12}$$

The drag force was approximated by the expression:

$$F_D = 6\eta \upsilon d \tag{4.13}$$

which is an equation valid for infinitely thin spheroids settling in random orientation [70].

By substituting Eqs. (4.11), (4.12) and (4.13) in the force balance for a particle settling under the influence of gravity as indicated in Eq. (4.6), the modified Stokes equation for oblate spheroids was then obtained:

$$d_{St}^{disc} = \sqrt{\frac{24R}{\pi}} \sqrt{\frac{\eta \nu}{(\rho_s - \rho_f) g}} \tag{4.14}$$

where d_{St}^{disc} is the modified Stokes diameter for discs.

By dividing Eq. (4.14) by Eq. (4.7) and rearranging one obtains the Pabst equation for determination of the average aspect ratio, $\overline{R}$:

$$\overline{R} = \frac{3\pi}{4} \left(\frac{D_{50}^L}{D_{50}^S} \right)^2 \tag{4.15}$$

where D_{50}^L is the median particle size obtained by laser diffraction and D_{50}^S is the median particle size obtained by sedimentation. Figure 4.6 is a graphical representation of equations (4.10) and (4.15). Even though equation (4.15) looks much simpler than

equation (4.10), it remarkably leads to practically the same results. It is important to emphasize that when D^L is a true disc diameter, which depends on whether the particle orientation is perpendicular to the laser beam or not, i.e., it depends on the hydrodynamic situation in the measuring cell, and can in principle be verified by microscopic image analysis, the aspect ratio R is indeed a true aspect ratio [71]. For the purpose of this investigation, D^L was considered as a true disc diameter.

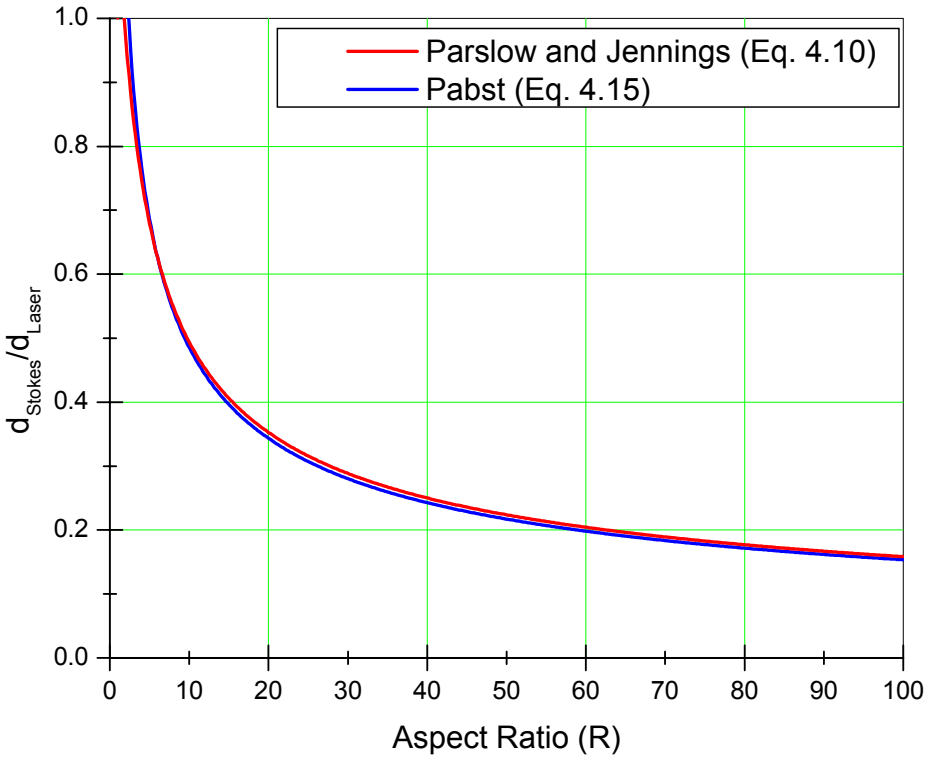

Figure 4.6. The variation of the ratio d_{Stokes} / d_{Laser} with aspect ratio for oblate spheroids using Parslow and Jennings and Pabst models.

As pointed out by Slepetys and Cleland [46], the light scattering instruments measure ESD related to the light scattering cross-section of particles. The light scattering cross-section is given by its geometrical cross-section multiplied by the scattering coefficients for the particle of interest. The scattering coefficients are in general functions of the refractive index and the direction of the particles [72]. In effect, one must multiply the projected geometrical cross-section in three principal directions with the corresponding scattering coefficient and then average the result.

As a first guess, van de Hulst [72] gave the scattering coefficients of sphere, rod and disc as functions of the refractive indexes and directions. In the specific case of light scattering by small particles compared to the wave length, he deduced the following relation of scattering coefficients (S):
for a sphere

$$S = \frac{3(m^2 - 1)}{(m^2 + 2)} \tag{4.16}$$

for a disc

$$S_{//} = m^2 - 1 \tag{4.17}$$

$$S_{\perp} = \frac{m^2 - 1}{m^2} \tag{4.18}$$

where ***m*** is the real component of the refractive index and $S_{//}$ and $S_{\perp}$ are the scattering coefficients along the long and short length of the particles, respectively. If it is assumed for the mean scattering coefficients of disc particles to be calculated from S = ($S_{//} + S_{\perp}$)/2 and considering ***m*** = 1.596 for talc, it follows that S_{sphere} = 1.0208 and S_{disc} = 1.0773. Since there is a relation, $d_{Stokes}/d_{Laser}.(S_{disc}/S_{sphere})^{1/2}$ = f(R), where $(S_{disc}/S_{sphere})^{1/2}$ is the correction coefficient as proposed by Slepetys and Cleland [46]. Introduction of the scattering coefficients into the relation gives:

for a disc

$$\left(\frac{D_{Stokes}}{D_{Laser}}\right) = 0.9734\, f(\mathrm{R}) \tag{4.19}$$

where f(R) stands for the function of R as described in equation (4.10). These calculations suggest that if one takes into consideration the direction dependence of scattering coefficients for non-spherical particles on evaluating aspect ratios, the

resultant aspect ratio values tend to decrease. Figure 4.7 shows a comparison between the Parlow and Jennings' model corrected and (Equation (4.19)) and the Pabst model (Eq.(4.15)).

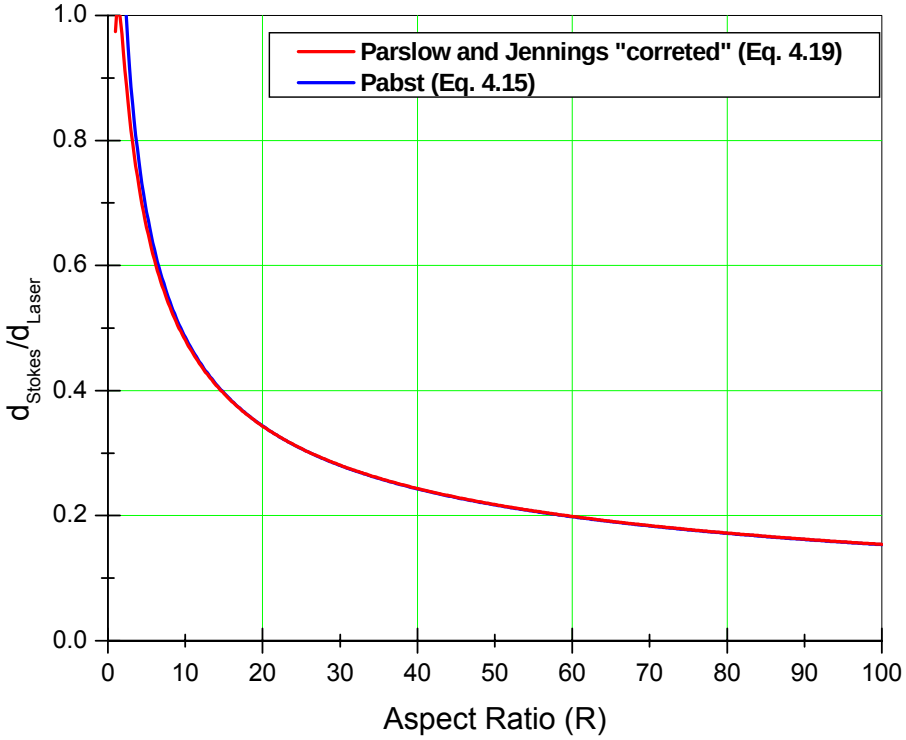

Figure 4.7. The variation of the ratio d_{Stokes} / d_{Laser} with aspect ratio for oblate spheroids using Parslow and Jennings corrected and Pabst models.

It can be concluded from the analysis of Figure 4.7 that after applying the Slepetys and Cleland coefficient the two models show an even better agreement for aspect ratios higher than about 10.

Figure 4.8 is a quantitative evaluation of the fit between the models. It shows that for the R ranging from 10 to 100 the average percentage difference between Pabst/J&P after the inclusion of the correction factor is only $\left|0.22\%\right|$ and without the correction the average difference is $\left|2.87\%\right|$. In the aspect ratio range from 2 to 10 the percentage difference is $\left|1.33\%\right|$ and $\left|4.1\%\right|$, respectively.

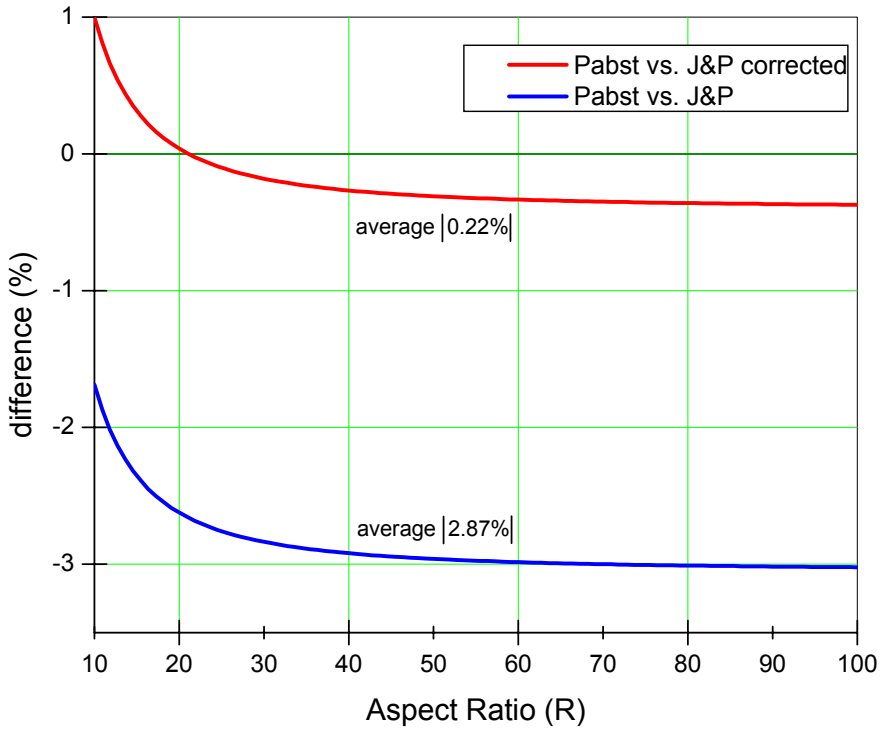

Figure 4.8. Percentage difference between the Pabst model and the Jennings and Parslow model with the correction coefficient (in red) and without the correction coefficient (in blue) in the aspect ratio range from 10 to 100.

4.5- Experimental procedure

A proper dispersion of the samples is the first and very critical step before proceed with the particle size analysis. The techniques employed here cannot distinguish between primary particles and clusters or agglomerates of particles and the presence of the latter will influence the accuracy of the measurements. Additionally, the refractive index of agglomerates is different from the one of individual particles of the same material. Thus, prior to the analysis the samples were thoroughly dispersed in distilled water with the help of 0.2 wt% sodium hexametaphosphate (dispersing agent) and an ultrasonic disruptor (200 W, 2 min.) to assure the individualization of the primary particles. The pH of the suspension was adjusted to 10.5 as a means of increasing the magnitude of the zeta potential of talc particles thus helping stabilizing the suspension.

Both instruments were calibrated by measuring the particle size distribution of polydisperse galss microspheres, a secondary particle size standard containing sizes ranging from 10 – 100 μm (PS-215, Whitehouse Scientific, Waverton, England).

The complex refractive index of talc considered for the laser diffraction analysis was N=1.596 + 0.1i. The density of the samples were individually determined using the procedure described in Section 1.7, Chapter 1.

For the understanding of the data shown in Table 4.1 below, the definition of some terms related to the laser diffraction technique is made necessary, that follows:

Median diameter D_{50}: the 50% volume percentile, expressed as d(*v*, 0.5) is also known as the median of the volume distribution. The *v* in the expression d(*v*, 0.5) shows that this refers to the volume distribution. This can be replaced by *s* for surface, *l* for length or *n* for number distributions.

Span: is the measurement of the width of the distribution which is independent of the median size. The smaller the value the narrower the distribution. The span of the distribution is defined as:

$$Span = \frac{d_{(x,0.9)} - d_{(x,0.1)}}{d_{(x,0.5)}} \tag{4.20}$$

The x is replaced by any of the letters *v, s, l, n* that define the distribution type. ***V*** for volume, ***s*** surface, ***l*** length and ***n*** number. The other term which describes the distribution type independently of the median size is the **uniformity**, which is a measure of the absolute deviations from the median.

Residual: is an indication of how closely the calculated data has been fitted to the measurement data and is expressed as a percentage. By examining the residual you

will be able to determine if the correct analysis mode or presentation has been chosen. A final residual of less than 1% indicates a good fit.

Obscuration: The obscuration helps set the concentration of the sample when it is added to the dispersant. It is the percentage or fraction of incident light that is attenuated due to extinction (scattering and/or absorption) by the particles . An ideal range is between 10 and 30%.

The complete report with the results of laser diffraction (Mie and Fraunhofer) and sedimentation analysis for each sample is presented on Appendix 1.

4.6- Comparison Mie versus Fraunhofer

In order to check the adequacy of the optical model used, for the coarsest and finest samples, A and H, both theories, Mie and Fraunhofer, were applied for the calculation of the scattered data. Figure 4.9 shows the comparison of the particle size distributions for sample A using both Mie and Fraunhofer models.

As described in the literature, there is a good agreement between the two theories for large particle sizes and this is indeed shown in Figure 4.9. On the other hand, for the finest sample, H, a significant difference between Mie and Fraunhofer was observed, as shown in Figure 4.10.

In this case Mie theory was considered to give the more accurate results since it is the most appropriate one for this size range. Table 4.1 compares Mie and Fraunhofer for all the other samples. Again there was a good agreement in the particle size distribution for all the samples but G and H which is an indication that the refractive index used for talc is rather reasonable. Since the Mie theory applies to the entire particle size range studied here, it was the one used for the determination of the diameters ratio ($d_{sedimentation}/d_{laser(Mie)}$) and consequently of the aspect ratio.

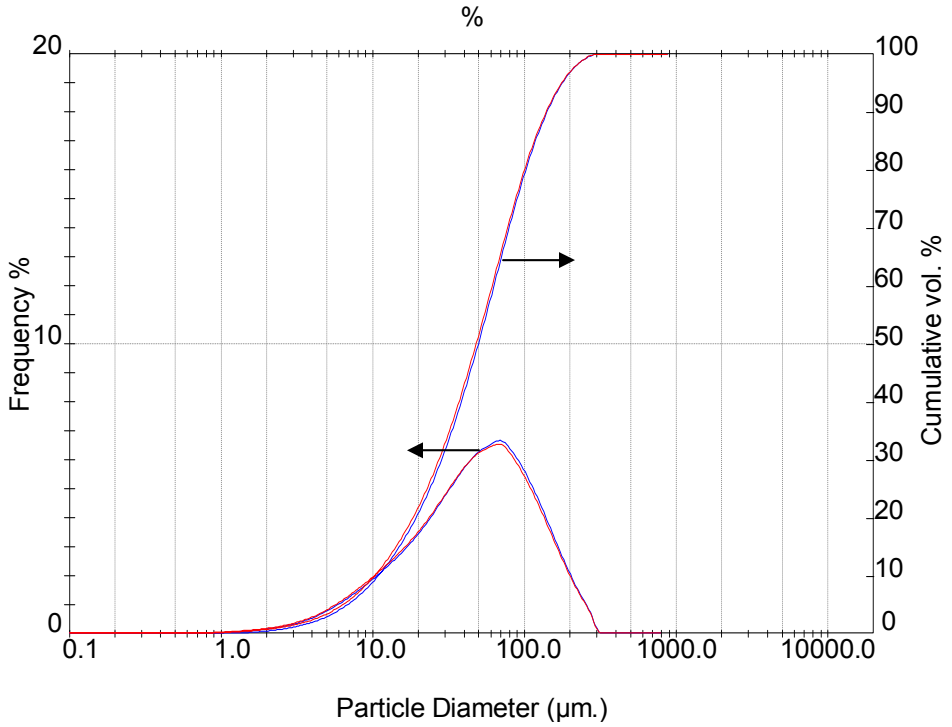

Figure 4.9. Comparison of Mie (blue line) and Fraunhofer (red line) optical models for coarse sample A.

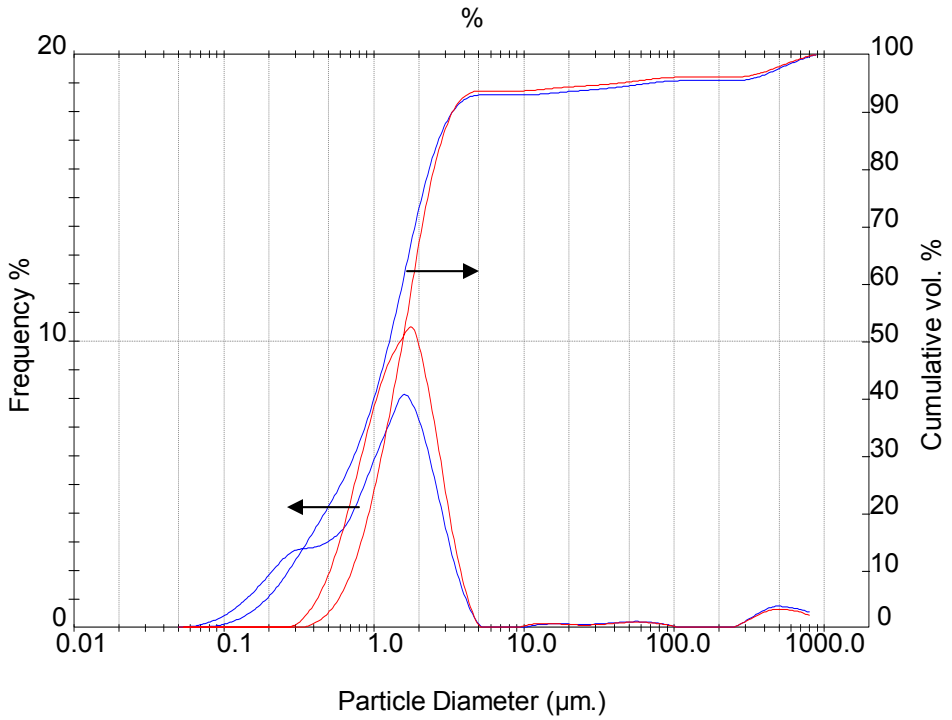

Figure 4.10. Comparison of Mie (blue line) and Fraunhofer (red line) optical models for fine sample H.

4.7- Results and discussion

Figure 4.11 compares gravitational sedimentation and laser diffraction data for the silica microspheres (PS-212, White House Scientific, UK) and shows that the results are in excellent agreement. Similar results have were reported by other authors for others isometric particles [69].

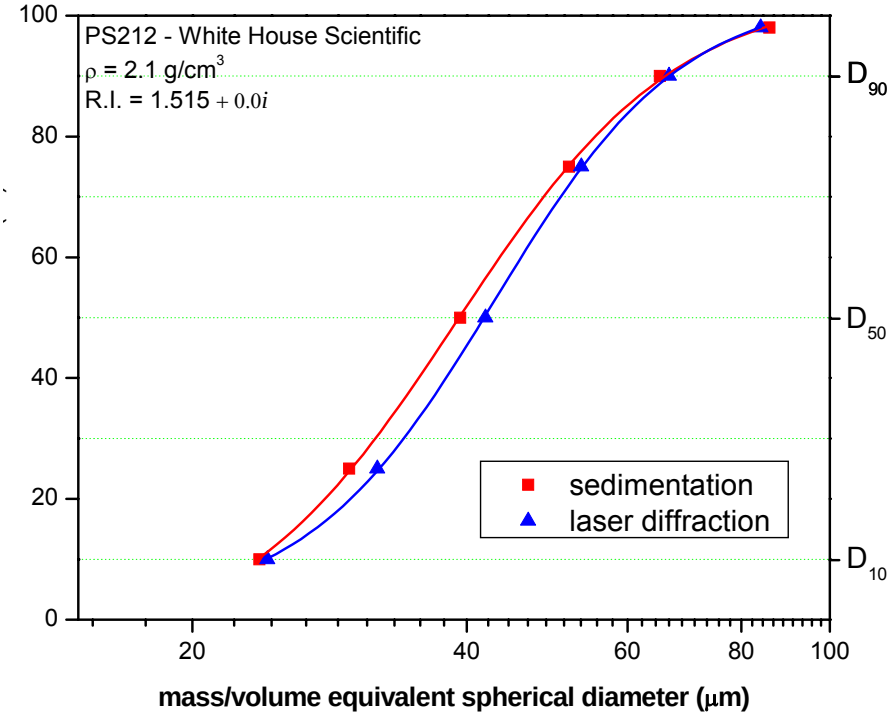

Figure 4.11. Comparison of particle size distribution results for spherical particles: sedimentation vs. laser diffraction.

This is a clear indication of the fact that the anisometry of particle shape, i.e. the deviation from sphericity, is the main factor responsible for large discrepancies between sedimentation and laser diffraction data. There is no doubt that the silica microspheres are by far more isometric than talc, i.e., their average aspect ratio will be much closer to unity. Figure 4.12 illustrates the regular morphology of the silica microspheres. Barreiros *et al.* [73] have also determined the diameter of glass beads using sedimentation, laser diffraction and microscopy and found practically the same value for the median diameter.

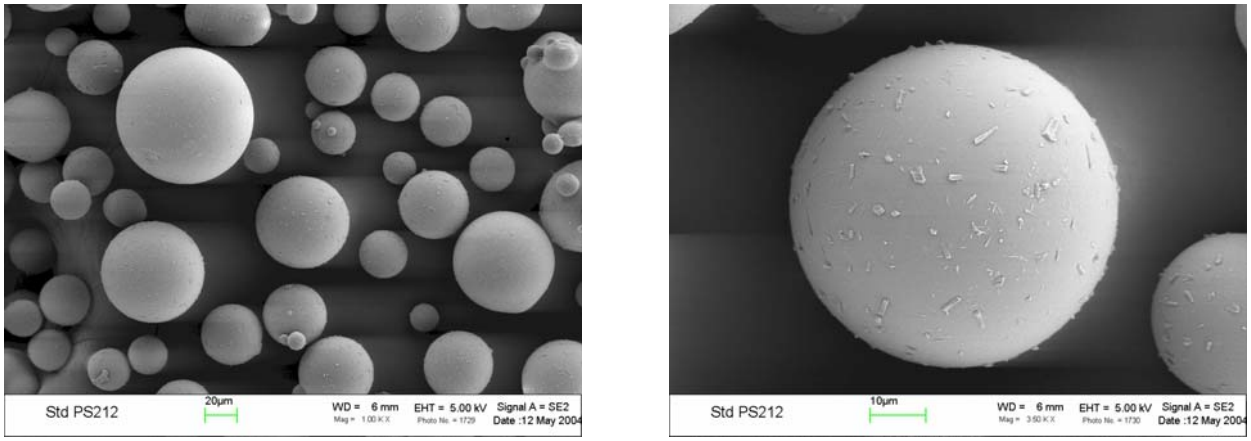

a-) b-)

Figure 4.12. Electron micrograph of silica microspheres (PS-212) used for equipment calibration: a-) 1000x; b-) 3500x.

Table 4.1 summarizes the data form the sedimentation and laser analysis. In the latter case, the results from both optical models Mie and Fraunhofer are presented. It also shows the calculated aspect ratios at different percentiles using the original Jennings and Parslow model Eq. (4.10), the corrected version Eq. (4.19) and the Pabst model Eq. (4.15). Finally, the degree of lamellarity, as defined by Eq. 1.1 (Chapeter 1) is also presented.

Table 4.1 contains some important observations. All of the materials studied here showed a wide range of distribution in size as given by the span; sample D was the one with the narrowest distribution (span=1.607) while sample G had the widest distribution (span=2.727).

As expected and described in section 4.4 (see Figure 4.5) the particle size distribution obtained by laser diffraction were invariably greater than those obtained by X-ray gravitational sedimentation. Distributions are not coincident for all the samples, but do follow the same profile. Figures 4.13 and 4.14 typify the shape of the curves and the expected divergence between the sedimentation and the laser diffraction.

Table 4.1. Summary data from particle size analysis and aspect ratio calculations

	SAMPLE →	A	B	C	D	E	F	G	H
sedimentation (gravitational)	d_{90} (μm)	52.80	33.90	13.58	3.94	3.83	3.06	1.20	0.80
	d_{50} (μm)	28.77	7.46	4.49	1.53	1.35	1.15	**0.49**	**0.39**
	d_{10} (μm)	7.21	1.24	**0.44**	**0.4**	**0.31**	**0.38**	**0.31**	**0.31**
laser (Mie)	d_{90} (μm)	140.56	55.7	39.39	12.02	9.97	8.96	5.11	3.44
	d_{50} (μm)	49.56	20.33	16.21	5.62	5.08	4.08	1.71	1.31
	d_{10} (μm)	10.82	5.14	4.71	2.12	2.22	1.4	0.31	0.28
	residual (%)	0.393	0.679	0.744	0.381	0.894	0.402	0.679	0.752
	span	2.617	1.891	2.101	1.886	1.607	1.802	2.727	2.423
	obscuration (%)	24.0	21.6	14.9	12.3	13.7	12.8	11.8	12.7
	uniformity	0.8092	0.586	0.6535	0.7069	0.5011	0.6706	10.08	20.61
laser (Fraunhofer)	d_{90} (μm)	138.67	54.89	38.83	12.71	11	8.64	4.77	3.36
	d_{50} (μm)	48.00	19.69	16.06	5.73	5.12	4.06	1.92	1.55
	d_{10} (μm)	10.22	4.83	4.44	2.07	1.86	1.5	0.83	0.71
	residual (%)	0.392	0.676	0.742	0.375	0.825	0.392	0.647	0.741
	span	2.676	2.542	2.141	1.856	1.784	1.759	2.052	1.703
	obscuration (%)	24.0	21.6	14.9	12.3	13.7	12.8	11.8	12.7
	uniformity	0.8275	0.7943	0.6660	0.6860	0.5549	0.642	7.723	14.49
Sed./Mie	$d_S/d_{L(90)}$	0.3756	0.6086	0.3448	0.3275	0.3839	0.3415	0.2348	0.2314
	$d_S/d_{L(50)}$	0.5805	0.3669	0.2770	0.2722	0.2657	0.2819	0.2865	0.2977
	$d_S/d_{L(10)}$	0.6664	0.2412	0.0934	0.1887	0.1396	0.2714	1.0000	1.1071
Parslow-Jennings (Eq. 4.8)*	R_{90}	17.6	6.4	20.9	23.2	16.8	21.3	45.4	46.7
	R_{50}	**7.1**	**18.4**	**32.5**	**33.7**	**35.4**	**31.4**	**30.4**	**28.1**
	R_{10}	5.2	43.0	287.3	70.3	128.6	33.9	1.0	n.d.
Parslow-Jennings corrected (Eq. 4.13)*	R_{90}	16.6	6.0	19.8	22.0	15.9	20.2	43.0	44.3
	R_{50}	**6.7**	**17.4**	**30.8**	**31.9**	**33.5**	**29.8**	**28.8**	**26.7**
	R_{10}	4.9	40.7	272.2	66.7	121.8	32.1	1.1	n.d.
Pabst (Eq. 4.9)*	R_{90}	16.7	6.4	19.8	22.0	16.0	20.2	42.7	44.0
	R_{50}	**7.0**	**17.5**	**30.7**	**31.8**	**33.4**	**29.6**	**28.7**	**26.6**
	R_{10}	5.3	40.5	270.1	66.2	120.9	32.0	2.4	1.9
Degree of lamellarity (Eq. 1.1)		0.7	1.7	2.6	2.7	2.8	2.5	2.5	2.4

*** From the ratio sedimentation/laser (Mie).**

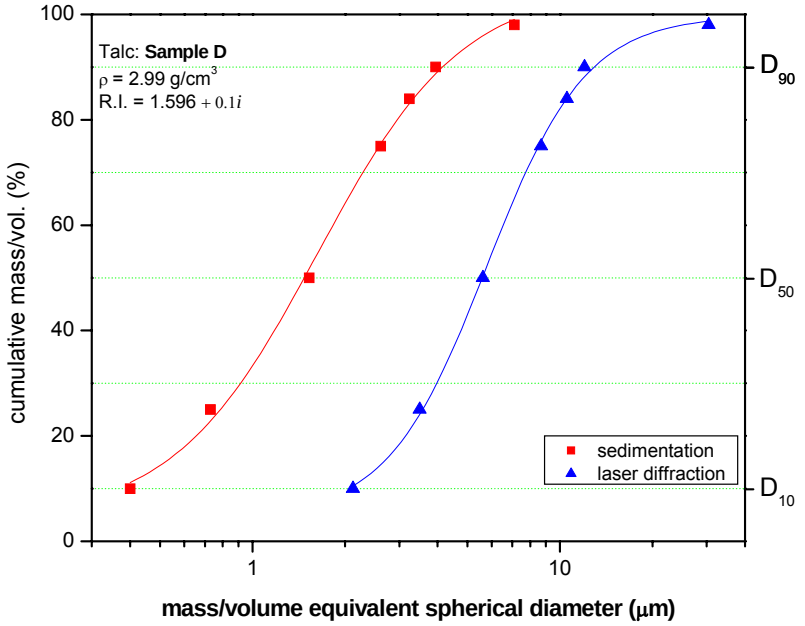

Figure 4.13. Particle size distributions of sample D measured by laser diffraction and sedimentation methods.

Sample D, Figure 4.13, represents the one in which the average aspect ratio, i.e., the aspect ratio calculated from the ratio of the corresponding median particle sizes (D_{50}) from each curve was the second highest (R = 31.9).

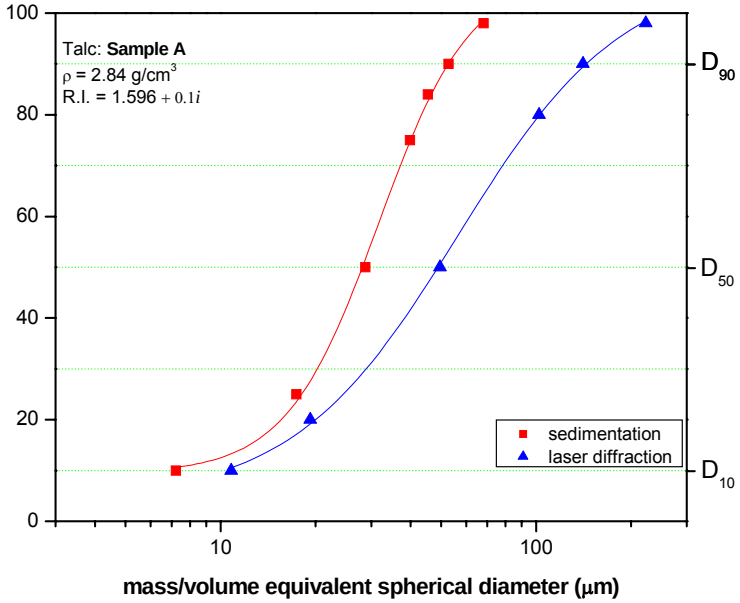

Figure 4.14. Particle size distributions of sample A measured by laser diffraction and sedimentation methods.

Sample A, Figure 4.14, was the one with the lowest average aspect ratio that can be observed from the proximity of the two curves in the region of D_{50}.

It is evident that a distribution of aspect ratio exists as a function of particle diameter. This distribution displays the following characteristic features: (1) the aspect ratios of samples A, G and H tend to decrease with increasing the particle diameters; (2) for other samples the inverse trend is observed, i.e, the aspect ratios increase with increasing in particle diameters. Inoue [30] reported that for a given sample of pyrophyllite (D_{50}^{Stokes} =4.2 μm), a phyllosilicate very similar to talc, the aspect ratio also increased with decreasing the particle diameters. Lohmander [48] also obtained increasing aspect ratios with decreasing particle diameters for talc.

From each curve, as the ones depicted in the figures 4.13 and 4.14, the 90%, 50% and 10% points of the cumulative frequencies gave the values of the characteristic diameters and are indicated in Table 4.1 for all samples. Using equation for oblate spheroids and the ratio $\frac{D_{sedimentation}}{D_{laser}}$, the aspect ratio data listed in the table were obtained. The minimum value obtained was for sample A (R=7) and the maximum was for sample E (R=33.4). A qualitative evaluation of the particles morphology was done by means of electronic microscopy. Typical electron micrographs for samples A and E are shown in Figures 4.15 and 4.16 below.

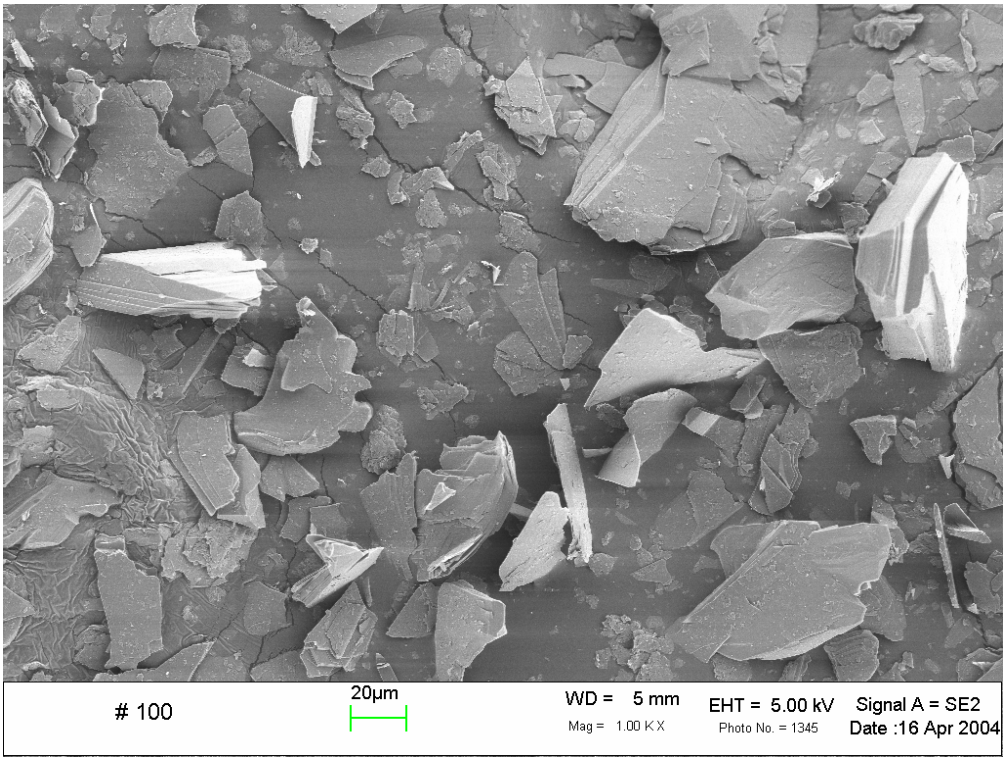

a-)

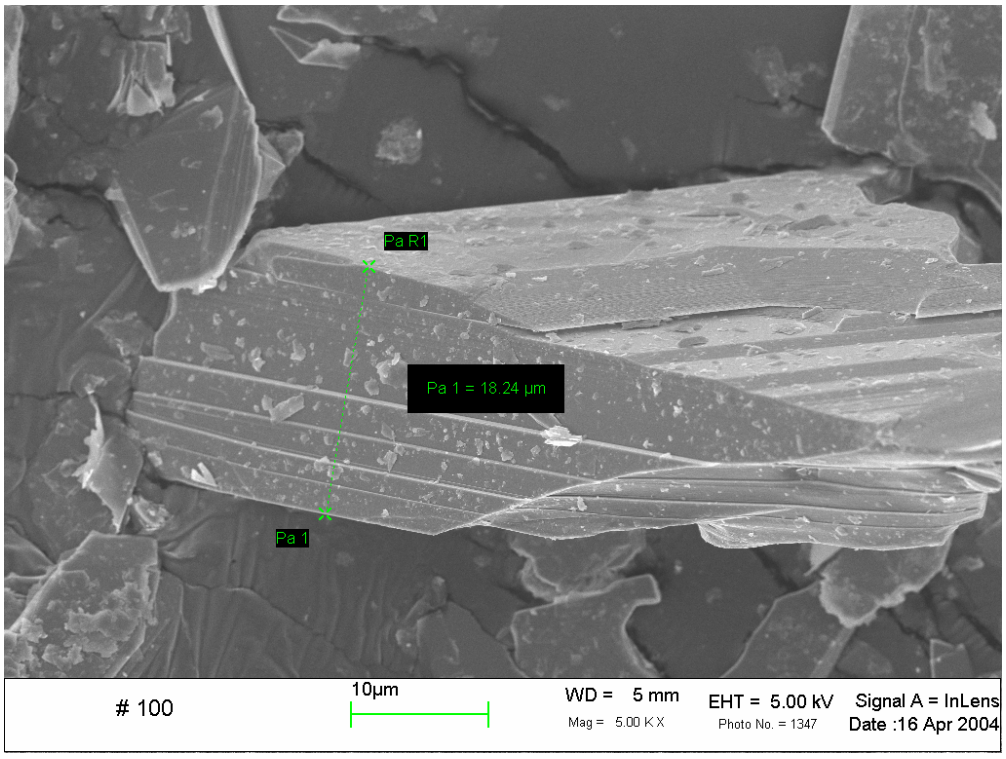

b-)

Figure 4.15. Electron micrograph of talc sample A: a-) 1000x; b-) 5000x.

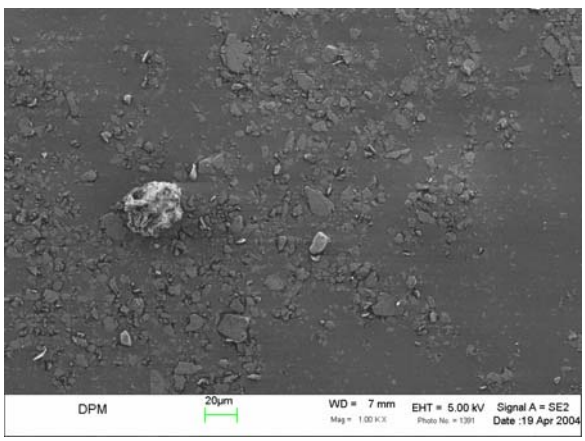

a)

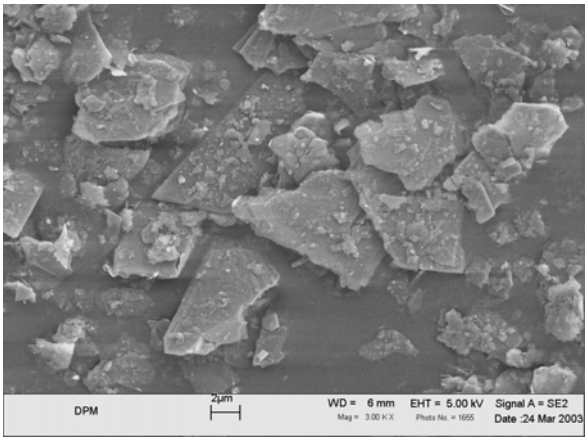

b)

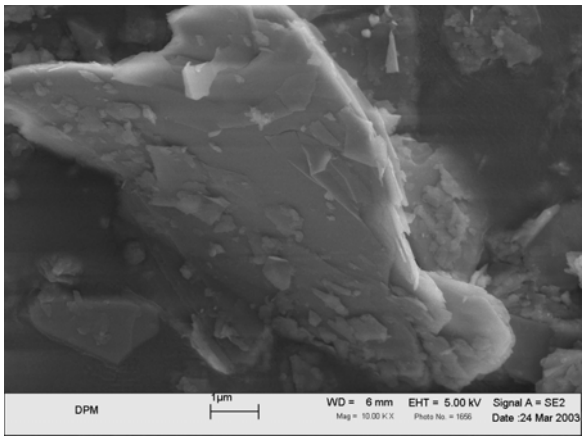

c)

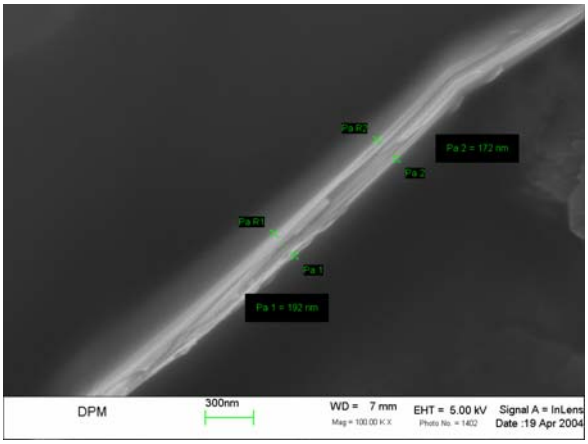

d)

Figure 4.16. Electron micrograph of talc sample E: a-) 1000x; b-) 3000x; c-) 10000x; d-) 100,000x.

The electron micrographs support the above observations. For the coarsest sample A, it is clear that the edge surfaces represent a great percentage of the total surface area and, consequently, the aspect ratio tends to be lower. On the other hand, the higher degree of delamination of sample E can be observed in Figure 4.16.

Table 4.1 also shows that there is a good agreement between the Mie and Fraunhofer theory for the coarsest samples (D_{50} > 5 μm, based on laser diffraction) and the discrepancy between the two optical models increases as the particles become finer and finer. This observation is in good agreement with data from literature [61]. The agreement between the optical models also indicates that the refractive index used for talc is very reasonable.

The results reveal that there is a good agreement in the aspect ratio as calculated by using the Jennings and Parslow equation and by using the Pabst equation. The agreement is even better when the correction factor first proposed by Slepetys and Cleland is applied.

The values corresponding to the average aspect ratio where plotted against the average particle size in Figure 4.17.

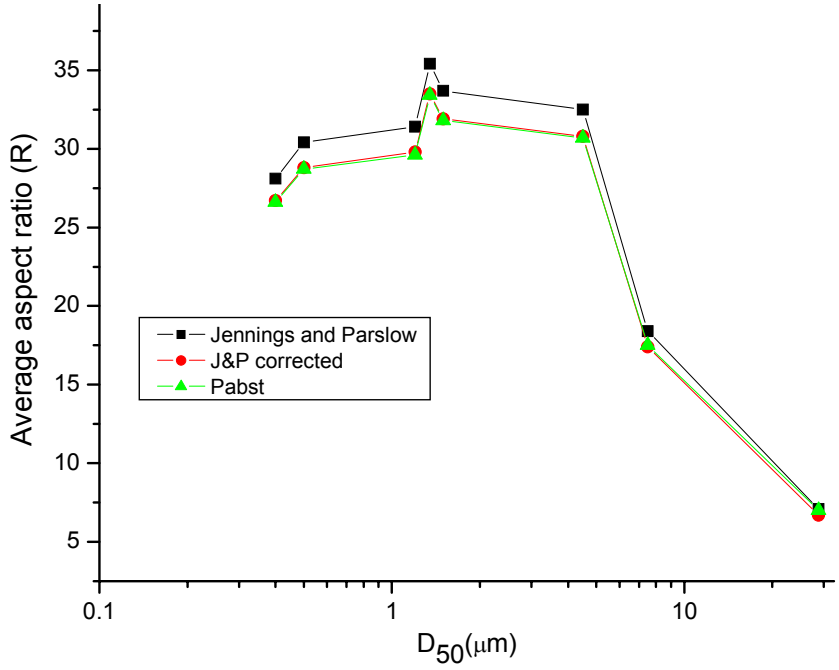

Figure 4.17. Average aspect ratio of talc samples as a function of average particle size.

Irrespective to the grinding technology used for this investigation, one might wish to argue that there is a limit in terms of maximum aspect ratio that can be achieved using the grinding technology applied in this investigation. For these specific talc samples, the delamination processes is efficient down to the average particle size (D_{50}, based on sedimentation) of about 4 μm. Then the delamination has a marginal increase in the average particle size range of about 4 – 1.0 μm. After that, below 1 μm, the evidence would appear to suggest that the fracture mechanisms prevail over delamination and the aspect ratio cannot be further increased. In other words, below 1 – 1.5 μm the size reduction of the particles will be accompanied by a significant

transverse breakage (parallel to the ***c-axis***) of the platelets giving rise to new lateral surfaces. As a result the overall hydrophilicity of talc increases and the contact angle with water decreases, as discussed in Chapter 3.

Similar results that support this hypothesis have been described in literature. Groszek [74], for example, showed that there was limit in the delamination of graphite, another lamellar mineral, in ball mill using increasing grinding times (Figure 4.18). The delamination in this case was inferred by the determination of the percentage of the hydrophobic basal plane areas of graphite by means of flow microcalorimetry.

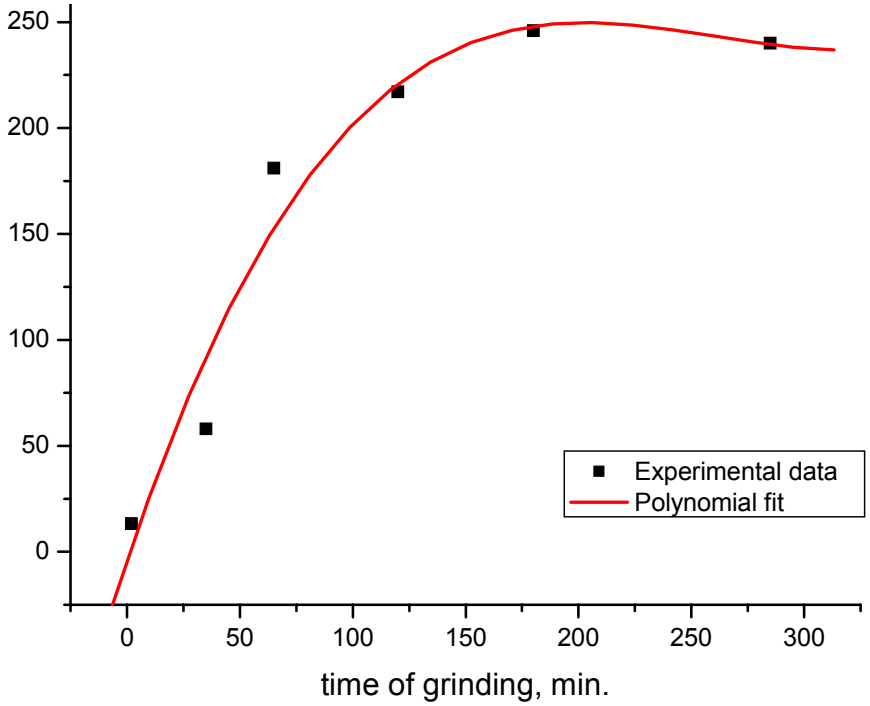

Figure 4.18. Change in the degree of delamination of graphite with grinding time. Reprinted with permission from ref. [74].

Ishimori and co-workers [32] used microscopy/image analysis combined with X-ray technique to determine the aspect ratio of talc. The delamination of the platelets was carried out using a laboratory-size ball mill and the maximum aspect ratio of 30 was achieved after a given grinding time (Figure 4.19). It is clear from their results that above the optimum grinding time the aspect ratio starts to decrease. They also concluded that delamination is predominant during the first stage of comminution and as

the particles become thinner, fracture is more noticeable. This same observation was described by other authors [75]. This not only confirms the hypothesis that there is limiting size for a maximum aspect ratio but also showed that the absolute value for the aspect ratio itself very similar to the average values shown in Table 4.1.

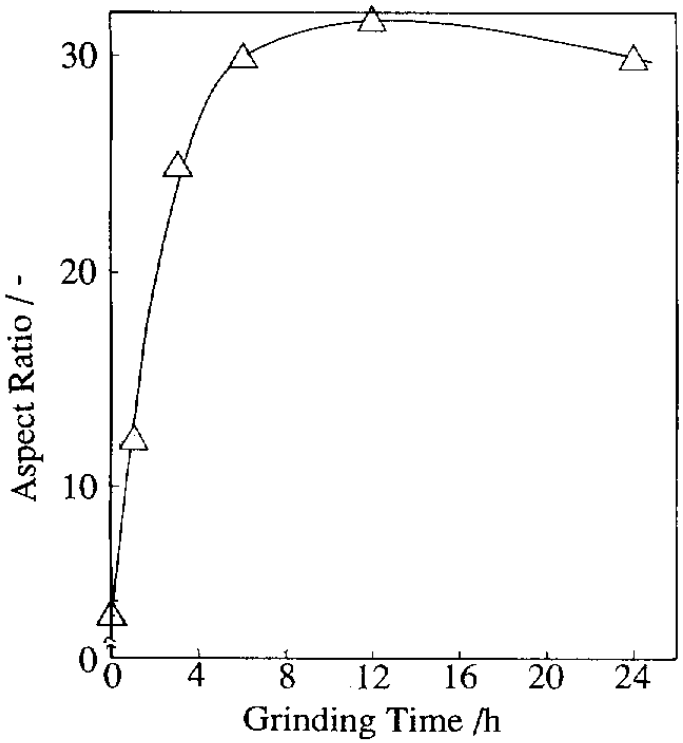

Figure 4.19. Variation of aspect ratio of talc with grinding time. The plate diameter was determined by microscopy with the aid of an image analyzer and the thickness from the X-ray crystallite size perpendicular to basal plane. Reprinted with permission from ref. [32].

Xanthos and co-workers [29] also achieved the same conclusion when working with mica which is another member of the phyllosilicate group of minerals. The curve of average aspect ratio as a function of grinding time showed a maximum and then the aspect ratio decreases with increasing grinding time.

Finally, the lamellarity index, as defined in Section 1.6 is listed in Table 4.1. Although the lamellarity index could be used to distinguish the samples in terms of the degree of delamination it is less sensitive than the value of the aspect ratio and it could be best viewed as a semi-quantitative indicator of the degree of delamination.

4.7.1- Microscopic analysis

As pointed out by some authors [30, 48], the geometrical particle sizes by imaging method are not directly comparable with the equivalent spherical diameters by the instrumental methods, because these techniques measure quite different parameters of individual particles. But comparison of these data provides at least an approximate guide to estimate their reliability. A brief microscopic evaluation of the aspect ratio was done with sample C (see Table 4.1). In total seven different particles showing a favorable orientation were randomly selected and their maximum diameter and thickness were measured with the help of image analysis software (LEO-32 V.02.03). Some examples of the electron micrographs with the respective diameter, thickness and aspect ratio for each individual particle are shown in Figure 4.20 a-f.

In total 7 particles were analyzed. An average aspect ratio/standard deviation of 28.4±7 was obtained. The maximum and minimum were 38.3 and 18.2, respectively. In order to have statistically meaningful result from SEM a much higher number of particles (~600) should have been measured. However, even though a direct comparison between the two techniques tends to diverge and the number of particles analyzed was very small, the numbers obtained by imaging analysis and particle size analysis are quite encouraging since they differ by only 8%.

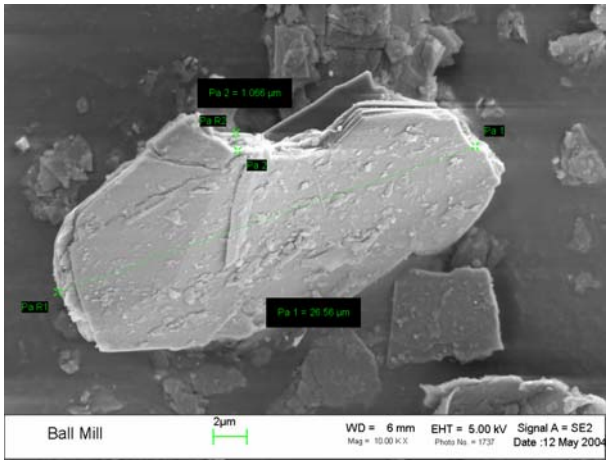

a-) ∅=26.56 µm; t=1.066 µm; **AR=24.9**

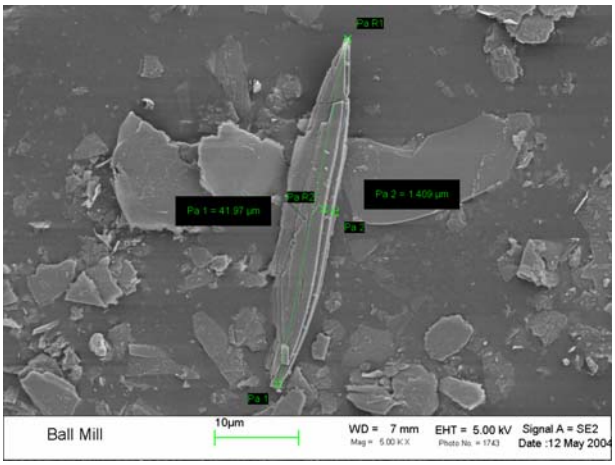

b-) ∅=41.97 µm; t=1.409 µm; **AR=29.8**

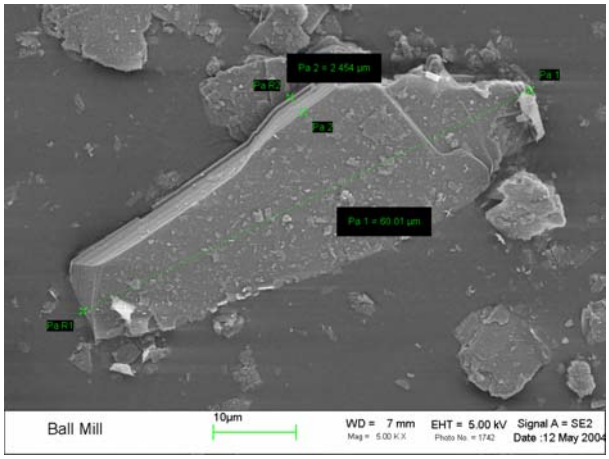

c-) ∅=60.01 µm; t=2.454 µm; **AR=24.5**

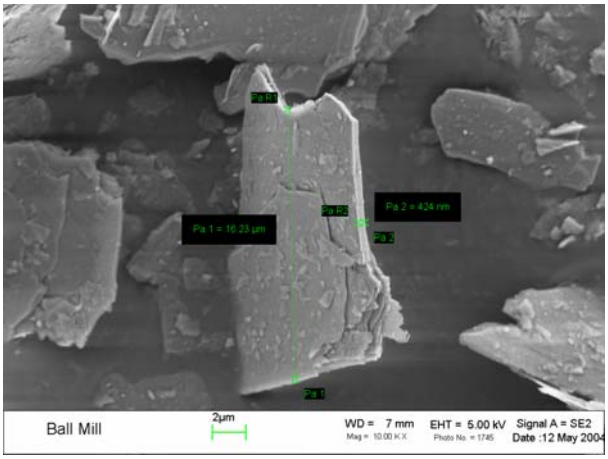

d-) ∅=16.23 µm; t=0.424 µm; **AR=38.3**

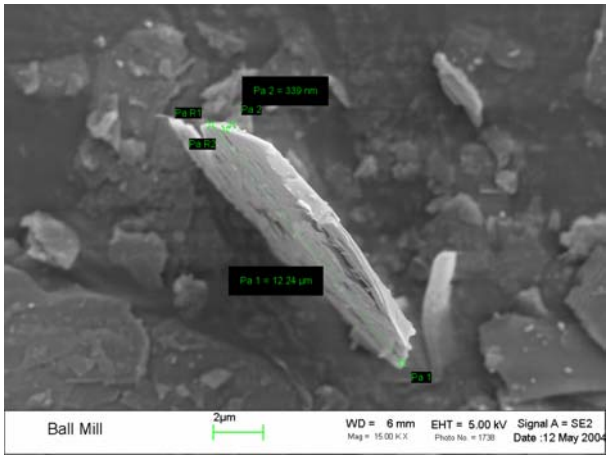

e-) ∅=12.24 µm; t=0.339 µm; **AR=36.1**

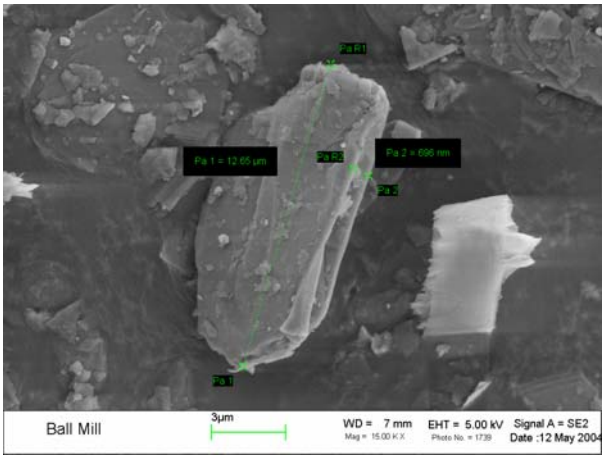

f-) ∅=12.65 µm; t=0.696 µm; **AR=18.2**

Figure 4.20. Determination of aspect ratio of sample C using scanning electron microscopy.

4.8- Conclusions

- The large discrepancy of the results of measurements of the particle size distributions by sedimentation and by laser diffraction is mainly caused by deviations of the particle shape from isometry. Therefore, the silica microspheres showed a very good agreement, whereas results from talc are usually significantly different for the two methods.

- Simple formulas are given for the aspect ratio, which may serve as a practical index of particle shape. Advantages of this method, compared with optical image analysis, are its low time consumption, its easy sample preparation, and the possibility to apply in connection with routine particle size measurements.

- It is suggested that using the grinding technology applied in this investigation there is a limit in terms of maximum delamination that can be achieved for talc.

- The method used for aspect ratio determination can be expected to work not only for talc, but for all powder systems with sufficiently anisometric particles in the size range where the physical principle of both sizing techniques are not violated.

4.9- References

1. Rothon, R.N. and M. Hancock, *The general principles guiding selection and use of particulate materials*, in *Particulate-filled polymer composites*, R.N. Rothon, Editor. 2003, Rapra Technology: Shropshire. p. 5-51.

2. Conley, R.F., *Attrition milling of industrial minerals*, in *Ultrafine Grinding and Separation of Industrial Minerals*, S.G. Malghan, Editor. 1983, Society of Mining Engineers: New York. p. 37-48.

3. Conley, R.F., *Effects of crystal structure and grinder energy on fine grinding of pigments.* Journal of Paint Technology, 1972. **44**(567): p. 67-84.

4. Hilbert, D. and S. Cohn-Vossen, *Geometry and Imagination*. 1st ed. 1952, New York: Chelsea.

5. Gotoh, K., *Particle shape characterization*, in *Powder Technology Handbook*, K. Gotoh, H. Masuda, and K. Higashitani, Editors. 1997, Marcel Dekker: New York. p. 43-56.

6. Hentschel, M.L. and N.W. Page, *Selection of descriptors for particle shape characterization.* Particle & Particle Systems Characterization, 2003. **20**: p. 25-38.

7. Clark, N.N. and T.P. Meloy, *Particle sample shape description with an automated Cascadograph particle analyser.* Powder Technology, 1988. **54**: p. 271-277.

8. Maine, F.W. and P.D. Shepherd, *Mica reinforced plastics: a review.* Composites, 1974: p. 193-200.

9. Canova, L.A. *Effects of aspect ratio on performance properties of mica reinforced polypropylene and nylon.* in *ANTEC 2000 Plastics: The Magical Solution.* 2000: Society of Plastics Engineers.

10. Nielsen, L.E. and R.F. Landel, *Particulate-filled polymers*, in *Mechanical properties of plymers and composites*. 1994, Marcel Dekker: New York. p. 386, 468.

11. Karrad, S., *et al., Influence of a fine talc on the properties of composites with high density polyethylene and polyethylen/polystyrene blends.* Journal of Membrane Science, 1998. **33**: p. 453-461.

12. Riley, A.M., *et al., Factors affecting the impact properties of mineral filled polypropylene.* Plastics and Rubber Processing and Applications, 1990. **14**: p. 85-93.

13. Liang, J.Z. and R.K.Y. Li, *Prediction of tensile yield strength of rigid inorganic particulate filled thermoplastic composites.* Journal of Materials Processing Technology, 1998. **83**: p. 127-130.

14. Bharadwaj, R.K., *Modeling the barrier properties of polymer-layered silicate nanocomposites.* Macromolecules, 2001. **34**: p. 9189-9192.

15. Lim, T.K., *Simplified model for the influence of inclusion aspect ratio on the stiffness of aligned reinforced composites.* Journal of Reinforced Plastics and Composites, 2003. **22**(4): p. 301-325.

16. Adams, J.M., *Particle size and shape effects in materials science: examples from polymer and paper systems.* Clay Minerals, 1993. **28**: p. 509-530.

17. Lohmander, S., *Influence of a shape factor of pigment particles on the rheological properties of coating.* Nordic Pulp and Paper Research Journal, 2000. **15**(3): p. 231-236.

18. Yuan, J. and H.H. Murray, *The importance of crystal morphology on the viscosity of concentrated suspensions of kaolins.* Applied Clay Science, 1997. **12**(3): p. 209-219.

19. Lohmander, S., *Influence of shape and shape factor of pigment particles on the packing ability in coating layers.* Nordic Pulp and Paper Research Journal, 2000. **15**(4): p. 300-305.

20. Morris, H.H., *et al.*, *Delaminated clays - physical and paper coating properties.* Tappi, 1965. **48**(12): p. 92A - 99A.

21. Lohmander, S., *The influence of particle shape of coating pigments on their packing ability and on the flow properties of coating colours*, in *Department of Pulp and Paper Chemistry and Technology*. 2000, KTH Royal Institute of Technology: Stockholm. p. 71.

22. Conley, R.F. *Statistical distribution patterns of particle size and shape in the Georgia kaolins*. in *Clays and Clay Minerals (Conference)*. 1966: Pergamon Press.

23. Nadeau, P.H., *The physical dimensions of fundamental clay particles.* Clay Minerals, 1985. **20**: p. 499-514.

24. Bundy, W.M. and J.N. Ishley, *Kaolin in paper filling and coating.* Applied Clay Science, 1991. **5**(5-6): p. 397-420.

25. Mahmud, F., *et al.*, *Measurement of shape and size distributions of PVC resin particles by scanning electron microscopy and image analysis.* European Polymer Journal, 1992. **28**(9): p. 1039-1043.

26. Zbik, M. and R.S.C. Smart. *Atomic force microscopy in the estimation of aspect ratio of colloidal kaolinite*. in *11th International Clay Conference*. 1997. Ottowa.

27. Zbik, M. and R.S.C. Smart, *Nanomorphology of kaolinites; comparative SEM and AFM studies.* Clays and Clay Minerals, 1998. **46**(2): p. 153-160.

28. Riley, C.M., *et al.*, *Quatitative shape measurements of distal volcanic ash.* Journal of Geophysical Research, 2003. **108**(B10): p. 8-1 - 8-15.

29. Kauffman, S.H., *et al.*, *The preparation and classification of high aspect ratio mica flakes for use in polymer reinforcement.* Powder Technology, 1974. **9**: p. 125-133.

30. Inoue, A., *Determination of aspect ratios of clay-sized particles.* Clay Science, 1995. **9**: p. 259-274.

31. Beckett, R., *et al.*, *Determination of thickness, aspect ratio and size distributions for platey particles using sedimentation field-flow fractionation and electron microscopy.* Colloids and Surfaces A: Physicochemical and Engineering Aspects, 1997. **120**(1-3): p. 17-26.

32. Ishimori, T., *et al.*, *Determination of geometrical properties of mechanically delaminated ultrathin talc platelets.* Particle & Particle Systems Characterization, 1994. **11**: p. 398-402.

33. Baudet, G., *et al.*, *Estimation of the average aspect ratio of lamellae-shaped particles by laser diffractometry.* Particulate Science and Technology, 1993. **11**: p. 73-96.

34. Bumiller, M.R. *Particle size of powder metals using laser diffraction*. in *International Conference and Exhibition on Powder Metallurgy and Particulate Materials*. 1993: American Powder Metallurgy Institute.

35. de Ridder, F., *et al.*, *Shape and size determination by laser diffraction: feasibility of data analysis by physical modeling.* Particle & Particle Systems Characterization, 2000. **17**: p. 195-205.

36. Ma, Z., *et al.*, *New developments in particle characterization by laser diffraction: size and shape.* Powder Technology, 2000. **111**(1-2): p. 66-78.

37. Ferrage, E., *et al.*, *Evaluation of talc morphology using FTIR and H/D substitution.* Clay Minerals, 2003. **38**: p. 141-150.

38. Bullman, V., *Automated three-dimensional analysis of particle measurements using an optical profilometer and image analysis software.* Journal of Microscopy, 2003. **211**: p. 95-100.

39. Parslow, K. and B.R. Jennings, *Simultaneous size and thickness measurements for heterogeneous micrometre-sized particles.* Journal of Physics D:Applied Physics, 1986. **19**: p. 1233-1243.

40. Jennings, B.R. and K. Parslow, *Particle size measurement: the equivalent spherical diameter.* Proceedings of Royal Society of London A, 1988. **419**: p. 137-149.

41. Jennings, B.R., *Size and thickness measurements of polydisperse clay samples.* Clay Minerals, 1993. **28**: p. 485-494.

42. Rawle, A., *Basic principles of particle-size analysis.* Surface Coatings International Part A, 2003(02): p. 58-65.

43. Allen, T., *Particle Size Measurement*. 4th ed. 1991, New York: Chapman and Hall.

44. Naito, M., *et al.*, *Effect of particle shape on the particle size distribution measured with commercial equipment.* Powder Technology, 1998. **100**(1): p. 52-60.

45. Novak, J., J. W. and J.R. Thompson, *Extending the use of particle sizing instrumentation to calculate particle shape factors.* Powder Technology, 1966. **45**(2): p. 159-167.

46. Slepetys, R.A. and A.J. Cleland, *Determination of shape of kaolins pigment particles.* Clay Minerals, 1993. **29**: p. 495-507.

47. Endoh, S., *et al.*, *Shape estimation of anisometric particles using size measurement techniques.* Particle & Particle Systems Characterization, 1998. **15**: p. 145-149.

48. Lohmander, S., *Aspect ratios of pigment particles determined by different methods.* Nordic Pulp and Paper Research Journal, 2000. **15**(3): p. 221-230.

49. Coakley, J.P. and J.P.M. Syvitski, *Sedigraph Technique*, in *Principles, methods, and application of particle size analysis*, J.P.M. Syvitski, Editor. 1991, Cambridge University Press: New Yorj. p. 129-142.

50. Allen, T., *A review of sedimentation methods of particle size analysis*, in *Particle Size Analysis*, N.G. Stanley-Wood and R.W. Lines, Editors. 1992, The Royal Society of Chemisry: Cambridge. p. 454 - 476.

51. *ISO 13317-1 - Determination of particle size distribution by gravitational liquid sedimentation methods - Part 1: General principles and guidelines*. 2001, International Organization for Standardization - ISO: Switzerland. p. 1-17.

52. Snow, R.H.*, et al.*, *Size reduction and size enlargement*, in *Perry's Chemical Engineers' Handbook*, D.W. Green, Editor. 1997, McGraw-Hill: New York. p. 20-1 - 20-89.

53. *ISO 13317-3 - Determination of particle size distribution by gravitational liquid sedimentation methods - Part 3: X-ray gravitational technique*. 2001, International Organization for Standardization - ISO: Switzerland. p. 1-11.

54. Jillavenkatesa, A.*, et al.*, *Particle Size Characterization*. Vol. Special publication 960-1. 2001, Washington: National Institute of Standards and Technology.

55. Allen, T. and M.G. Baudet, *The limits of gravitational sedimentation.* Powder Technology, 1977. **18**(2): p. 131-138.

56. Allen, T., *Sedimentation techniques of particle size measurement*, in *Particle Size Analysis 1985*, P.J. Lloyd, Editor. 1987, John Wiley and Sons: Chichester. p. 25-45.

57. *Malvern Mastersizer Manual*. 1997, Malvern Instruments: Worcestershire, UK.

58. Xu, R., *Particle size distribution analysis using light scattering*, in *Liquid- and Surface-borne Particle Measurement Handbook*, J.Z. Knapp, T.A. Barber, and A. Lieberman, Editors. 1996, Marcel Dekker: New York. p. 745-777.

59. *ISO 13320-1 - Particle size analysis - Lase diffraction methods - Part 1: General principles*. 1999, International Organization for Standardization - ISO: Switzerland. p. 1-34.

60. de Boer, G.B.J.*, et al.*, *Laser diffraction spectrometry: Fraunhofer Diffraction versus Mie Scattering.* Particle Characterization, 1987. **4**: p. 14-19.

61. Mackinnon, I.D.R.*, et al.*, *Kaolinite particle size in the < 2 ìm range using laser scattering.* Clays and Clay Minerals, 1993. **41**(5): p. 613-623.

62. Palik, E.D., *Handbook of Optical Constants of Solids*. !st ed. 1985, Orlando: Academic Press.

63. *CRC Handbook of Chemistry and Physics*. 83 ed, ed. D.R. Lide. 2002: CRC Press.

64. Bohren, C.F. and D.R. Huffman, *Absorption and sacttering of light by small particles*. 1st ed. 1983, New York: John Wiley and Sons.

65. Xu, R., *Particle Characterization: Light Scattering Methods*. 1st ed. 2002, New York: Kluwer Academic Publishers.

66. Rawle, A., *Malvern Instruments, MA, USA. Personal communication*. 2004.

67. *ISO 14887 - Sample preparation - dispersing procedures for powders in liquids*. 2000, International Organization for Standardization - ISO: Switzerland. p. 1-24.

68. Jones, R.M., *Particle size analysis by laser diffraction: ISO 13320, standard operating procedures and Mie theory.* American Laboratory, 2003: p. 44-47.

69. Pabst, W., *et al., A note on particle size analyses of kaolins and clays.* Journal of the European Ceramic Society, 2000. **20**(9): p. 1429-1437.

70. Pabst, W., *et al., Extraction of shape information from particle size measurements.* British Ceramic Transactions, 2001. **100**(3): p. 106-109.

71. Pabst, W., *Department of Glass and Ceramics (ICT Prague). Personal Communication.* 2004.

72. van de Hulst, H.C., *Light Scattering by Small Particles*. 1st ed. 1957, New York: Dover Publications.

73. Barreiros, F.M., *et al., Calculating shape factors from particle sizing data*. Particle & Particle Systems Characterization, 1996. **13**: p. 368-373.

74. Groszek, A.J., *Selective adsorption at graphite/hydrocarbon interfaces.* Proceedings of Royal Society of London A, 1970. **314**: p. 473-498.

75. Baudet, G., *et al., Two dimensions comminution of kaolinite clay particles.* Powder Technology, 1999. **105**(1-3): p. 125-134.